Supporting Information for:

Hydrogen Storage Properties and Neutron Scattering Studies of Mg$_2$(dobdc)—A Metal-Organic Framework with Open Mg^{2+} Adsorption Sites

Kenji Sumida,[a] Craig M. Brown,[b]* Zoey R. Herm,[a] Sachin M. Chavan,[c] Silvia Bordiga,[c] and Jeffrey R. Long [a]*

[a]Department of Chemistry, University of California, Berkeley, California 94720, USA, Lawrence Berkeley National Laboratory, Berkeley, CA 94720, USA

[b]Center for National Institute of Standards and Technology, Center for Neutron Research, Gaithersburg, MD 20899, USA

[c]Department of Chemistry, IFM & NIS Centre of Excellence, University of Torino, Via Quarello, 11 I-10135 Torino, Italy

email: jrlong@berkeley.edu, craig.brown@nist.gov

Chem. Commun.

Experimental Details

General Considerations. All reagents were obtained from commercial vendors and used without further purification. All manipulations, unless otherwise stated, were performed in air.

Synthesis and activation of Mg$_2$(dobdc). The literature procedure[1] was adapted. H$_4$dobdc (0.56 g, 2.8 mmol) and Mg(NO$_3$)$_2$·6H$_2$O (2.4 g, 9.3 mmol), DMF (220 mL), ethanol (15 mL), and water (15 mL) were added to a 500 mL conical flask, and the mixture was sonicated until dissolution of the solid reagents. The mixture was then dispensed into 25 × 20 mL scintillation vials, and tightly capped with Teflone-lined caps. The vials were then placed on a hot plate at 120 °C, and heated for a period of 8 h. The resulting solid was then combined, and transferred to a dinitrogen-filled glove box. The material was submerged in anhydrous DMF (50 mL), and heated at 80 °C for a period of 2 days, replacing the DMF each 12 h. The DMF was decanted, and replaced with methanol (50 mL). The suspension was heated to 100 °C for a period of 3 days, replacing the methanol each 12 h. The material was activated by heating the solid *in vacuo* to a temperature of 180 °C at a ramp rate of 0.2 °C/min to afford 0.35 g (51 %) of desolvated product.

Infrared Spectra. Infrared spectroscopic measurements were performed using a custom-made cryogenic cell that allows: (i) *in-situ* high-temperature activation of the sample under a high vacuum and (ii) variable-temperature infrared spectroscopy of the adsorbed species while simultaneously measuring temperature and equilibrium pressure. For infrared spectroscopy, a thin self-supported wafer of the sample was prepared and activated under high vacuum (residual pressure <10^{-4} mbar) at 433 K for 18 h. Transmission FTIR spectra were collected, at 2 cm^{-1} resolution on a Bruker Equinox-55 FTIR spectrometer equipped with an MCT detector.

A series of IR absorption spectra recorded over a sufficiently large temperature range while simultaneously measuring temperature and equilibrium pressure of the adsorbed gas, allows the standard adsorption enthalpy and entropy to be determined by following the variable-temperature infrared method. Here, integrated absorbance (*A*) of an infrared absorption band characteristic of a gas adsorption complex, temperature (*T*) and equilibrium pressure (*p*) are considered to be interrelated by the Langmuir type equation:

$$\theta = A/A_M = K(T)p/[1 + K(T)p] \tag{1}$$

where θ stands for the fractional coverage of (localized) adsorption sites, A_M is the integral IR absorbance corresponding to full coverage ($\theta = 1$), and K is the adsorption equilibrium constant at temperature, T. Combination of eq. 1 with the van't Hoff (eq. 2) leads to eq. 3 below;

$$K(T) = \exp(-\Delta H^0/RT) \exp(\Delta S^0/R) \tag{2}$$

$$\ln[A/(A_M - A)p] = (-\Delta H^0/RT) + (\Delta S^0/R) \tag{3}$$

After determining the relative band intensity from the integrated infrared absorbance as a function of T and p, eq. 3 gives direct access to the standard adsorption enthalpy (ΔH^0) and entropy (ΔS^0). It should be noted, however, that knowledge of A_M is needed. From that approximate value (for each of the adsorbed gases), we obtained the corresponding refined values of A_M by following the iteration procedure described elsewhere.[2]

Upon lowering the temperature below 80 K, (Fig. S4a), a new band grows at 4127 cm^{-1}, followed by another component at 4137 cm^{-1}. This spectral range is typical of weakly perturbed hydrogen interacting with the organic framework.[3,4] The band at 4127 cm^{-1} can be assigned to the second adsorption site identified by neutron diffraction, while the band at 4137 cm^{-1} is attributed to physisorbed hydrogen. As this component appears at lower temperature it comes out that the adsorption enthalpy involved is lower than the main adsorption site (Mg^{2+}). A quantitative evaluation of adsorption enthalpy cannot be made as this band is developing together with the high frequency component at 4137 cm^{-1} due to physisorbed hydrogen.

Keeping the sample at 20 K the band at 4085 cm^{-1} progressively decreases in intensity in favor of the component centered at 4091 cm^{-1} (Fig. S4b). Similarly, the band at 4127 cm^{-1} disappears and a complex absorption at the low frequency side, with a maximum of 4137 cm^{-1} is present (from red to black curve). This behavior can be explained in terms of ortho-para conversion of adsorbed hydrogen on both sites. This explanation is confirmed by the spectra evolution upon lowering the equilibrium pressure, as shown in Fig. S4c. All the components show a progressive decrease in intensity as a function of equilibrium pressure, following their stability trend. The high frequency component is the first to disappear, followed by the band at 4135 cm^{-1} (black curves) and finally by the doublet at 4091 cm^{-1} and 4085 cm^{-1} (blue curves).

Note that in desorption the intensity ratio of this doublet (blue curves) is opposite to that observed during the adsorption (see Fig. 4), as expected in presence of ortho-para conversion.

Powder Neutron Diffraction. The powder diffraction patterns were measured at 4 K using the BT-1 diffractometer at the National Institute of Standards and Technology Center for Neutron Research (NCNR). An activated sample of Mg_2(dobdc) (1.89 g) was loaded in a vanadium cell equipped with a capillary gas line and a packless valve, and sealed with an indium O-ring. The sample was mounted onto a sample stick, equipped with a stainless-steel gas line with an additional valve for a top loading closed-cycle helium refrigerator (CCR). Using a wavelength of 2.078 Å and collimation of 15', powder patterns were recorded for the bare material and at nominal loading values of 0.6 D_2, 1.2 D_2, and 2.4 D_2 per Mg^{2+} site. During the experiments, a known amount of hydrogen (deuterium) gas was loaded into the sample, which was maintained at a temperature of 70 K until no pressure drop could be observed for at least 1 minute. The sample was then cooled down to the base temperature of the CCR (4 K) over one hour in order to perform measurements. In all cases the outgas pressure reading was zero well before reaching 25 K. Data collection times at 4 K were for approximately 11 h.

Neutron scattering diffraction patterns were analyzed using the Rietveld refinement method with the program EXPGUI.[5] The model of the bare material, based on that of previous work,[6] was refined first and it was used as the starting point for subsequent refinements of the D_2-loaded samples. Fourier difference maps were used to successively determine the missing nuclear density from the added D_2. In the refinements, deuterium molecules are treated as point scatters with double occupancy since they are quantum mechanically rotationally averaged in the ground state.[7] The deuterium adsorbed at the metal site was able to be refined with anisotropic thermal parameters, while the higher adsorption sites were refined isotropically. Final refinements at the highest loading were performed with anisotropic thermal parameters for all deuterium.

Inelastic Neutron Scattering (INS). The INS spectra were measured at 4 K using the pyrolytic graphite monochromator and 20'-20' collimation options on the BT-4 filter analyzer neutron spectrometer (FANS)[8] at the NCNR. The sample (1.286 g) was sealed in a cylindrical aluminum cell suitable for *in-situ* gas loading while cooled in a CCR.

Hydrogen gas was used during the measurements to take advantage of its large incoherent neutron scattering cross section. A H_2 molecule is a very good quantum rotor due to its light mass and consists of two indistinguishable fermions (protons) that require the wavefunction to be *anti*-symmetric. If the nuclear spins of two protons are anti-parallel, H_2 is said to be in a *para* state (*p*-H_2); otherwise, it is in an *ortho* state (*o*-H_2). The quantum rotation number, J, of a H_2 molecule thus has to be even for a *para*-H_2 and odd for an *ortho*-H_2. At room temperature, only one fourth of H_2 molecules are in the *para* state. Usually, the conversion rate between states is very slow, but can be greatly accelerated in the presence of a fluctuation magnetic moment. Normal hydrogen (*n*-H_2) consisting of 25 % *p*-H_2 and 75% *o*-H_2 was used in these experiments.

A neutron scattered by a H_2 molecule can induce the required nuclear spin flip to convert a *para*/*ortho* H_2 to an *ortho*/*para* H_2. This *para*-*ortho* or *ortho*-*para* transition is associated with the change of the rotational quantum number, J, from even/odd to odd/even, and has a large neutron scattering cross-section that is proportional to the incoherent neutron scattering cross-section of the proton. INS spectra of the adsorbed H_2 were obtained by subtracting the INS spectrum of the bare materials. For a free hydrogen molecule, the *para*-*ortho* transition is usually associated with the $J = 0$ to $J = 1$ excitation occurring with an energy of 14.7 meV, which can be directly measured by INS but not optical spectroscopies. The local potential of a host material will generate rotational barriers for the adsorbed H_2 which typically cause the $J = 1$ state to split into its three sublevels. Additionally, the translation excitations of the H_2 molecule may be coupled to the rotational transition and complicate the observed spectra. Hence, the INS spectra of adsorbed H_2 may show complex features with multiple peaks in the spectrum containing rich information about the host material and the hydrogen interactions.

Loadings of 0.2, 0.4 and 0.6 *n*-H_2 per Mg^{2+} site were performed at 70 K with data collection at 4 K. Additional measurement at 0.2, 0.4, 0.6 and 1.2 loadings were also performed using *p*-H_2 after evacuating the system of H_2 at room temperature. Data were collected for approximately 9 h per loading. The energy resolution is between 1.2 meV to 2.0 meV over the energy transfer ranges accessible.

Background measurements of unloaded and activated parent Mg_2(dobdc) and Zn_2(dobdc) compounds were made to higher energy transfers (35 meV to 125 meV) using a copper monochromator with 20'-20' collimation before and after the monochromator resulting in an

energy resolution that degrades from 1.2 meV to 3 meV with increasing energy transfer. Data from the two monochromators are normalized to merge around 37 meV. Data reduction, including the subtraction of the bare $Mg_2(dobdc)$ spectrum from the hydrogen loaded spectra, and peak fitting were performed within the DAVE software suite.[9]

Quasielastic Neutron Scattering (QENS). The QENS spectra were measured using the Disk Chopper Spectrometer (DCS)[10] at the NCNR. QENS measurements using an instrument configured for the highest neutron flux at a wavelength of 5.0 Å. With detectors masked that contained Bragg peaks, and grouped in momentum transfer (Q) with 0.2 Å^{-1} bins, this instrument configuration allows for an accessible Q range of 0.27 Å^{-1} to 2.27 Å^{-1} with an elastic energy resolution of approximately 110 meV.

An activated sample of $Mg_2(dobdc)$ sample (1.286 g) was mounted in a CCR. As with the other experiments, the sample can was connected with a stainless steel capillary line to a gas-handling unit consisting of a reference volume and a high-resolution pressure transducer. Normal hydrogen loading was performed at 77 K at select pressures along the hydrogen isotherm. These correspond to H_2:Mg loadings of 0.33, 0.86, 0.95, 1.21, 1.42 and 1.57. Scattering from $Mg_2(dobdc)$ without H_2 was also measured at 77 K to serve as a background and subtracted from the loaded data.

An additional series of data were collected at a shorter wavelength of 1.81 Å using the medium resolution configuration of the disk chopper slits. The accessible Q-range is grouped in bins of 0.3 Å^{-1} between 0.75 Å^{-1} to 5.82 Å^{-1} with an elastic energy resolution of approximately 1 meV. In this case data were collected at 4 K for the bare $Mg_2(dobdc)$ and the same after loading with 1.2, 2.0, and 2.6 p-H_2 per Mg site. Data reduction, including vanadium normalization, the subtraction of the bare $Mg_2(dobdc)$ spectrum from the hydrogen loaded spectra, masking of detectors containing Bragg peaks, and peak fitting were performed within the DAVE software suite.[7]

Accessible Surface Area Calculation. The source code for the accessible surface area calculation program was obtained free of charge from the Internet.[11] The crystallographic information file (CIF) obtained from the single crystal X-ray structure was converted to the XYZ file format using Mercury CSD 2.0. The XYZ file and UFF force field atomic parameters[12] were

used as input for the simulation (atomic diameters (Å): H 2.571, C 3.431, N 3.260, O 3.118, Mg 2.691), and the accessible surface area was evaluated using a dinitrogen-sized probe molecule (diameter = 3.681 Å) inserted at randomized points in the unit cell, and averaging the resultant individual accessible surface area values after 5000 trials.

Note: Identification of commercial equipment or products in the text is not intended to imply any recommendation or endorsement by the National Institute of Standards and Technology.

Table S1. N_2 adsorption isotherm for an activated sample of $Mg_2(dobdc)$ at 77 K.

P (P/P$_0$)	N_2 adsorbed (mmol/g)
0.000000878	0.45196
0.000000504	0.90398
0.000000381	1.35596
0.000000322	1.80798
0.000000308	2.26004
0.000000339	2.71208
0.000000439	3.16414
0.000000549	3.61618
0.000000715	4.06823
0.000000964	4.52028
0.000001449	4.97225
0.00000245	5.4242
0.000004302	5.87604
0.0000068	6.32772
0.000009532	6.77918
0.000013114	7.23047
0.000017705	7.68159
0.000022853	8.13244
0.000028581	8.58304
0.000035145	9.03334
0.000042962	9.48325
0.000052599	9.93269
0.000065289	10.38148
0.000082907	10.82941
0.000109084	11.27592
0.000150384	11.72025
0.000217982	12.16093
0.000328359	12.59556
0.000497811	13.02085
0.000741452	13.43274
0.001074248	13.8265
0.001645689	14.26789
0.002597467	14.70359
0.004394724	15.12391
0.00802908	15.50733
0.015397123	15.84146
0.026767365	16.08788
0.041813593	16.27488
0.059298271	16.41762
0.079139954	16.53514
0.099392183	16.62889
0.120250013	16.70732
0.187650281	16.89734
0.28199433	17.08621

Table S1 (continued)

P (P/P$_0$)	N$_2$ adsorbed (mmol/g)
0.365179576	17.22543
0.45523533	17.35961
0.544346183	17.48665
0.63380921	17.60935
0.72284072	17.70903
0.811458196	17.78112
0.898494709	17.87059
0.365179576	17.22543
0.45523533	17.35961
0.544346183	17.48665
0.63380921	17.60935
0.72284072	17.70903
0.811458196	17.78112
0.898494709	17.87059

Table S2. H_2 adsorption and desorption data in an activated sample of Mg_2(dobdc) at low pressure.

T = 77 K		T = 87 K	
P (mmHg)	H_2 adsorbed (wt %)	P (mmHg)	H_2 adsorbed (wt %)
0.01609	0.00874	0.06813	0.00830
0.01684	0.00949	0.07337	0.00902
0.02328	0.01477	0.08251	0.01028
0.02708	0.01828	0.09368	0.01184
0.03457	0.02503	0.12048	0.01555
0.04036	0.03015	0.1386	0.01802
0.04985	0.03847	0.18251	0.02397
0.0608	0.04806	0.25251	0.03328
0.07446	0.05989	0.34311	0.04499
0.09218	0.07460	0.61094	0.07753
0.11471	0.09244	1.1711	0.13810
0.13334	0.10652	1.36291	0.15681
0.17621	0.13692	1.5661	0.17562
0.2534	0.18564	1.77175	0.19377
0.31285	0.21865	1.98042	0.21127
0.57141	0.33264	2.82356	0.27421
1.10856	0.48276	3.65853	0.32684
1.30108	0.52067	8.11928	0.51238
1.53131	0.55927	12.56733	0.61967
1.79199	0.59620	15.69557	0.67306
1.93386	0.61395	20.65212	0.73764
2.76227	0.69405	25.41906	0.78440
3.55134	0.74717	37.46127	0.86815
8.77762	0.91131	49.33936	0.92582
14.17155	0.98610	74.70584	1.01165
20.73193	1.04466	98.13953	1.06982
28.66537	1.09683	150.7119	1.16828
38.18626	1.14693	202.3772	1.24390
49.48042	1.19668	253.2031	1.30713
73.8224	1.28451	305.8827	1.36503
96.54567	1.35278	355.1409	1.41383
149.9381	1.48406	399.9669	1.45474
202.2384	1.58808	449.725	1.49701
253.6657	1.67520	499.8202	1.53661
305.5979	1.75179	549.9237	1.57351
357.7301	1.81989	600.2042	1.60851
399.8606	1.86978	650.1652	1.64105

(Table S2, continued)

T = 77 K		T = 87 K	
P (mmHg)	H$_2$ adsorbed (wt %)	P (mmHg)	H$_2$ adsorbed (wt %)
450.3966	1.92428	699.9309	1.67226
500.7569	1.97385	750.9542	1.70268
549.9459	2.01857	799.8884	1.73102
599.7507	2.06045	841.1624	1.75369
649.6672	2.10029	887.2121	1.77860
700.0921	2.13762		
749.8715	2.17224		
800.3763	2.20529		
838.2482	2.22880		
883.4202	2.25586		

Table S3. Higher-pressure H_2 adsorption data in activated Mg_2(dobdc) at 77 K.

P (bar)	Adsorption	
	Excess Uptake (wt %)	Total Uptake (wt %)
0.4032	1.70753	1.72177
2.15692	2.54329	2.58951
4.68462	2.88683	2.97911
7.65319	3.04501	3.19132
11.04632	3.11632	3.32432
14.51782	3.13044	3.40148
18.01872	3.11863	3.45316
21.57513	3.07628	3.47523
25.13807	3.05285	3.51625
28.7598	3.02368	3.5525
32.38153	2.99171	3.58588
35.99999	2.99515	3.65452
39.64132	2.99953	3.72442
43.2761	2.98313	3.77334
46.95009	3.01387	3.87001
50.6404	3.03799	3.96027
54.3405	3.08104	4.06956
57.86099	3.13345	4.18489
61.61335	3.08296	4.20139
65.36571	3.04003	4.22536
69.13113	3.04135	4.29372
72.94228	3.05792	4.37805
76.84812	3.03976	4.42923
80.74744	3.09656	4.55517
84.70228	3.08746	4.61609
88.65057	3.12928	4.72772
92.65113	3.17157	4.84063
96.75294	3.14318	4.88456

Table S4. Higher-pressure H_2 adsorption data in an activated sample of Mg_2(dobdc) at 298 K.

P (bar)	Excess Uptake (wt %)	Total Uptake (wt %)
14.5864	0.09693	0.16784
19.43932	0.12723	0.21859
29.21048	0.18642	0.31895
38.92938	0.22288	0.39631
43.86068	0.25443	0.44853
58.51088	0.31621	0.57187
78.18708	0.37947	0.71776
97.80778	0.42091	0.84148

Table S5. Unit cell parameters, unit cell volume and goodness of fit parameter for refinements.

Numbers in parentheses indicate one standard deviation in the final digit.

D_2 loading	a (Å)	c (Å)	V (Å^3)	Goodness of fit χ^2
0	25.861(3)	6.9143(8)	4005.0(7)	1.30
0.6 D_2/Mg	25.844(3)	6.9232(7)	4004.7(7)	1.24
1.2 D_2/Mg	25.842(2)	6.9283(7)	4007.0(6)	1.11
2.4 D_2/Mg	25.860(3)	6.9347(9)	4016(1)	1.26

Table S6. Refined occupancies and close contact distances for D_2 in Mg_2(dobdc). Numbers in parentheses indicate one standard deviation in the final digit.

Nominal loading D_2	Refined amount D_2	Site I –Mg^{2+} (Å)	Site I-Site II (Å)	Site III – Site I (Å)	Site IV- Site II (Å)
0.6 D_2/Mg	**1.16(7)** site 1: 0.89(3) site 2: 0.27(4)	2.45(4)	2.90(10)		
1.2 D_2/Mg	**1.98(11)** site 1: 0.99(4) site 2: 0.85(5) site 3: 0.14(2)	2.43(4)	3.16(8)	2.92(9)	-
2.4 D_2/Mg	**3.7(2)** site 1: 1.02(5) site 2: 1.00(5) site 3: 0.75(5) site 4: 0.92(3)	2.40(6)	3.23(8)	2.99(8)	3.11(9)

Table S7. Rietveld refinement for an evacuated sample of Mg_2(dobdc). Numbers in parentheses indicate one standard deviation in the final digit.

	x	y	z	Occupancy	U_{iso}(Å^2)	Multiplicity
Mg	0.3823(14)	0.3482(16)	0.1347(40)	1	0.057(9)	18
O1	0.3245(13)	0.2911(14)	0.3546(49)	1	0.042(10)	18
O2	0.2990(16)	0.2256(15)	0.5963(46)	1	0.069(10)	18
O3	0.3560(12)	0.2789(12)	-0.0105(44)	1	0.042(9)	18
C1	0.3177(17)	0.2463(14)	0.3985(52)	1	0.11(1)	18
C2	0.3323(14)	0.2080(11)	0.2904(44)	1	0.060(10)	18
C3	0.3469(14)	0.2288(13)	0.0774(42)	1	0.062(9)	18
C4	0.35052(98)	0.1784(12)	-0.0253(31)	1	0.037(6)	18
H	0.36106	0.18445	-0.18163	1	0.037	18

Table S8. Rietveld refinement for a sample of Mg_2(dobdc) after a dosing of 0.6 D_2 per Mg^{2+} site. Numbers in parentheses indicate one standard deviation in the final digit.

	x	y	z	Occupancy	U_{iso}(Å^2)	Multiplicity
Mg	0.3811(16)	0.3509(16)	0.1318(57)	1	0.075(16)	18
O1	0.3264(11)	0.2916(12)	0.3552(43)	1	0.021(10)	18
O2	0.3041(14)	0.2265(13)	0.5921(48)	1	0.056(12)	18
O3	0.3522(12)	0.2741(16)	-0.0039(48)	1	0.031(9)	18
C1	0.3149(17)	0.2489(17)	0.4251(49)	1	0.100(14)	18
C2	0.3240(14)	0.2056(17)	0.2657(61)	1	0.064(10)	18
C3	0.3423(15)	0.2252(18)	0.0726(61)	1	0.065(11)	18
C4	0.34912(98)	0.1774(20)	-0.0160(37)	1	0.056(10)	18
H	0.36106	0.18445	-0.18163	1	0.037	18
D1	0.2022(10)	-0.0106(12)	0.0613(29)	1.776(61)	0.185*	18
D2	0.4921(35)	0.1228(32)	0.009(14)	0.538(65)	0.312(89)	18

* Anisotropic thermal parameters for D1:
[U_{11}, U_{22}, U_{33}, U_{12}, U_{13}, U_{23}]=[0.23(4), 0.26(3), 0.07(2), 0.16(3), -0.06(2), -0.02(2)]

Table S9. Rietveld refinement for a sample of Mg_2(dobdc) after a dosing of 1.2 D_2 per Mg^{2+} site

	x	y	z	Occupancy	U_{iso}(Å^2)	Multiplicity
Mg	0.3767(16)	0.3496(16)	0.1499(60)	1	0.056(12)	18
O1	0.3249(12)	0.2932(12)	0.3585(32)	1	0.009(7)	18
O2	0.3060(14)	0.2286(13)	0.5939(35)	1	0.024(7)	18
O3	0.3534(12)	0.2749(14)	-0.0109(38)	1	0.013(7)	18
C1	0.3107(14)	0.2422(13)	0.4099(36)	1	0.049(9)	18
C2	0.3259(16)	0.2074(16)	0.2732(49)	1	0.058(11)	18
C3	0.3442(15)	0.2215(17)	0.0741(42)	1	0.047(9)	18
C4	0.35024(99)	0.1803(12)	-0.0261(30)	1	0.020(6)	18
H	0.36106	0.18445	-0.18163	1	0.037	18
D1	0.2012(12)	-0.0153(14)	0.0724(29)	1.97(8)	0.221*	18
D2	0.4998(13)	0.1262(14)	-0.0047(61)	1.7(1)	0.24(2)	18
D3	0.7469(49)	0.2354(45)	0.150(18)	0.27(4)	0.04(4)	18

* Anisotropic thermal parameters for D1:
[U_{11}, U_{22}, U_{33}, U_{12}, U_{13}, U_{23}]=[0.28(4), 0.35(4), 0.03(1), 0.21(3), -0.06(2), -0.04(2)]

Table S10. Rietveld refinement for a sample of $Mg_2(dobdc)$ after a dosing of 2.4 D_2 per Mg^{2+} site

	x	y	z	Occupancy	$U_{iso}(Å^2)$	Multiplicity
Mg	0.3733(25)	0.3540(26)	0.2032(83)	1	0.09(3)	18
O1	0.3277(18)	0.2873(20)	0.3418(66)	1	0.02(1)	18
O2	0.2975(17)	0.2192(18)	0.6023(53)	1	0.015	18
O3	0.3486(23)	0.2713(21)	-0.0226(71)	1	0.056(17)	18
C1	0.3154(17)	0.2485(22)	0.4527(75)	1	0.052	18
C2	0.3193(16)	0.2039(20)	0.2853(74)	1	0.038(14)	18
C3	0.3396(21)	0.2223(25)	0.0750(87)	1	0.082(20)	18
C4	0.3504(13)	0.1739(25)	-0.0114(55)	1	0.038(11)	18
H	0.3629	0.1947	-0.1791	1	0.013	18
D1	0.2035(15)	-0.0124(19)	0.0889(43)	2.04(9)	0.33*	18
D2	0.5095(22)	0.1166(21)	0.0286(52)	2.0(1)	0.32*	18
D3	0.7507(26)	0.2423(20)	0.1951(47)	1.51(9)	0.2*	18
D4	0.6240(24)	0.2420(14)	0.0106(45)	1.83(6)	0.32*	18

* Anisotropic thermal parameters
D1: $[U_{11}, U_{22}, U_{33}, U_{12}, U_{13}, U_{23}]$=[0.24(3), 0.63(5), 0.13(2), 0.38(3), -0.03(2), -0.02(2)]
D2: $[U_{11}, U_{22}, U_{33}, U_{12}, U_{13}, U_{23}]$=[0.43(5), 0.27(3), 0.30(3), 0.16(3), -0.16(4), -0.11(3)]
D3: $[U_{11}, U_{22}, U_{33}, U_{12}, U_{13}, U_{23}]$=[0.14(4), 0.20(3), 0.18(3), 0.04(2), -0.04(3), -0.01(4)]
D4: $[U_{11}, U_{22}, U_{33}, U_{12}, U_{13}, U_{23}]$=[0.22(4), 0.36(4), 0.42(5), 0.11(4), 0.03(4), 0.10(3)]
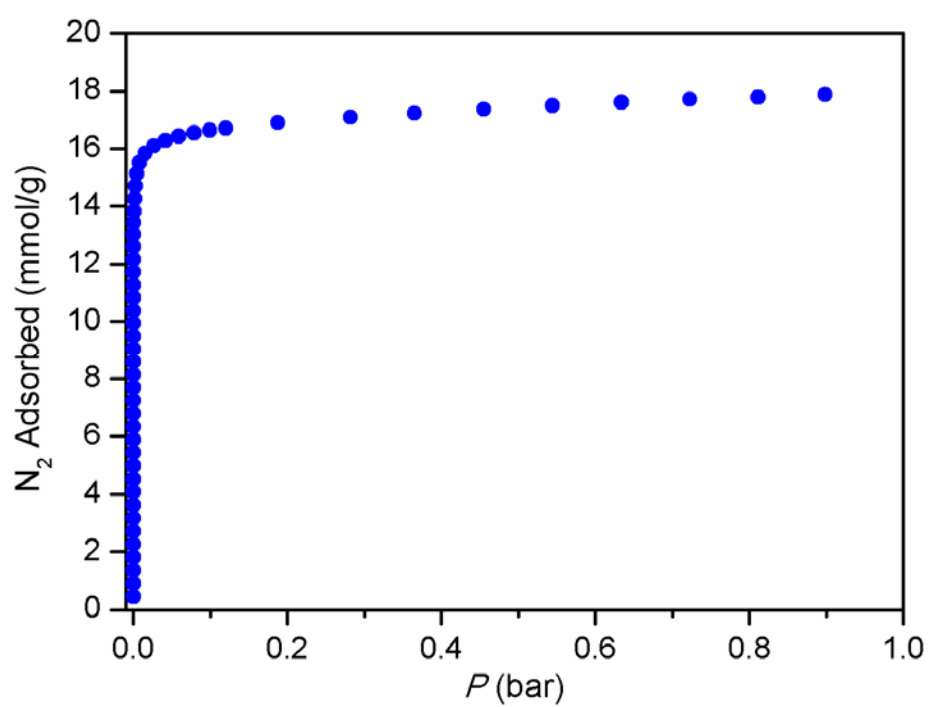
Figure S1. N_2 adsorption isotherm in an activated sample of $Mg_2(dobdc)$ recorded at 77 K.

slope = 2.887×10^{-3}
intercept = 3.522×10^{-7}
c = 8197.5
V$_m$ = 346.36
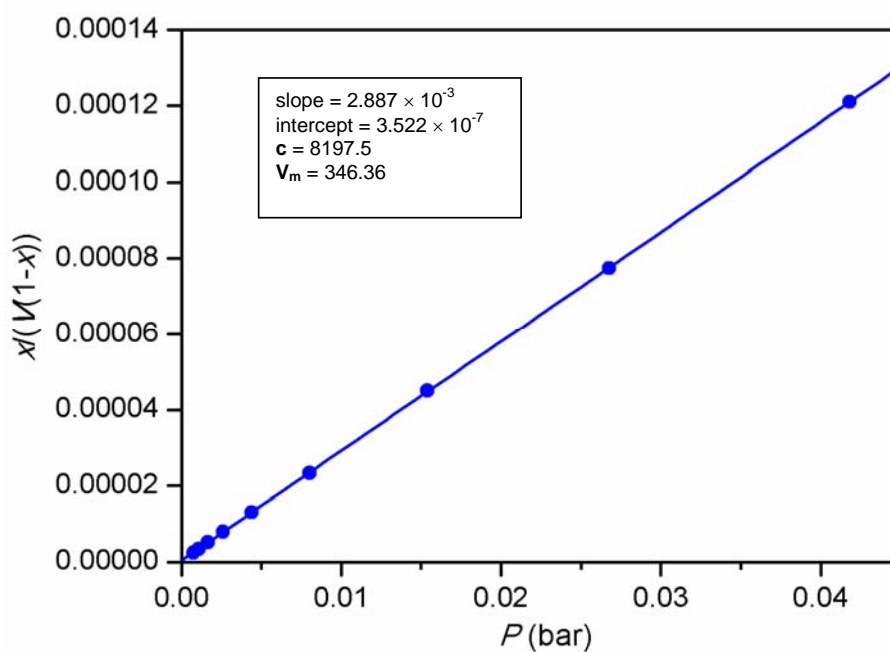
Figure S2. A BET plot of the adsorption isotherm for N_2 in Mg_2(dobdc) at 77 K, where x represents the quantity (P/P$_0$) and V is the volume of N_2 adsorbed. The blue line represents a linear best fit of the data points. Inset: parameters for the linear best fit and resulting constants for calculation of the BET surface area.
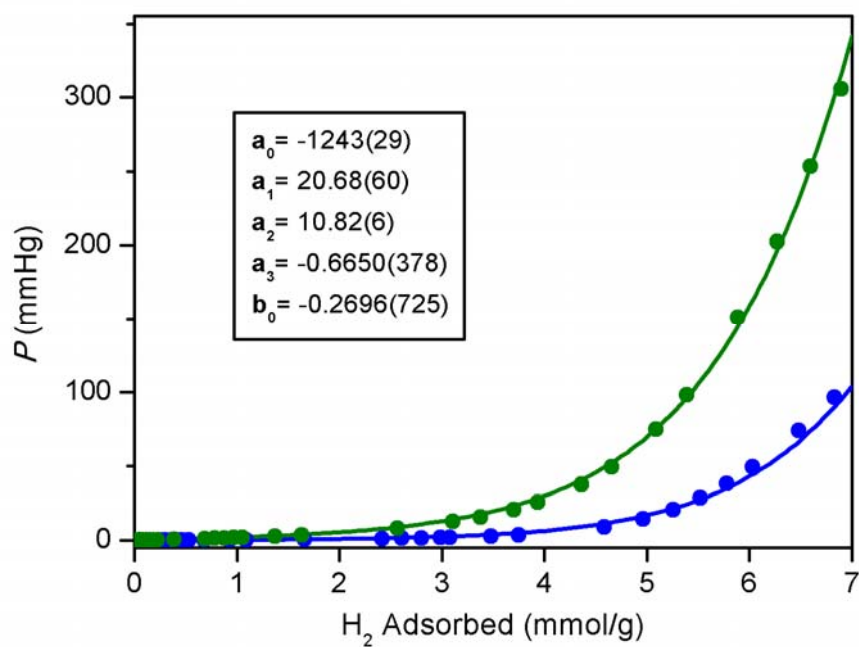
Figure S3. Fitting of the hydrogen adsorption data recorded at 77 K (blue) and 87 K (green) using a virial type function. Inset: virial parameters used for the fitting to the data.
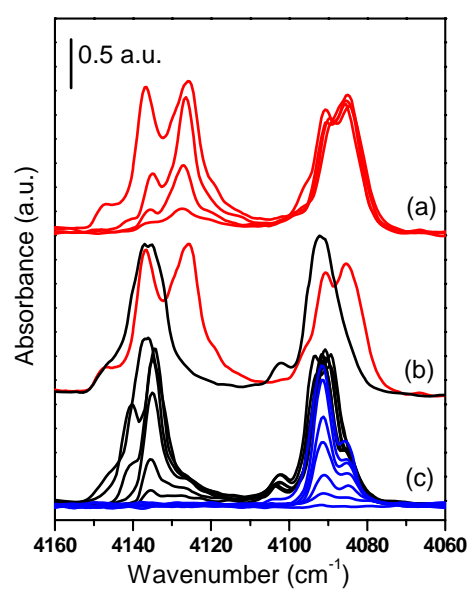
Figure S4. Infrared spectra of H_2 adsorbed on activated $Mg_2(dobdc)$. (a) effect of decreasing temperature in the range 80-20 K, (b) spectra evolution as function of time at 20 K: red curve initial time; black curve after 12 h, (c) progressive lowering of H_2 equilibrium pressure at 20 K, from black to blue curves.
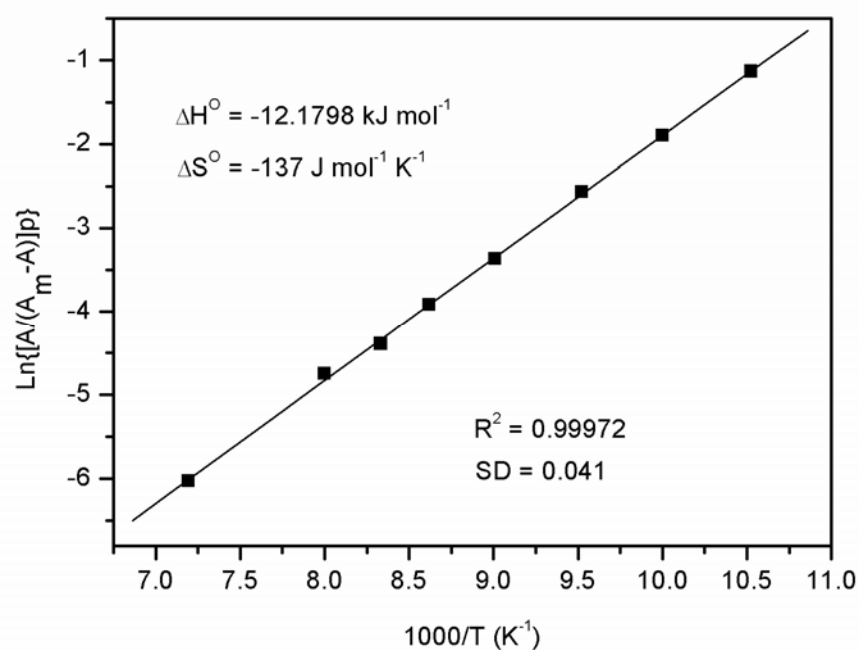
Figure S5. A van't Hoff-type plot derived from the integrated infrared absorption intensity for H_2 adsorbed within Mg_2(dobdc), where A is the integrated absorbance, A_m is the integrated absorbance at full coverage ($\theta = 1$), p is the equilibrium pressure, and T is the temperature.
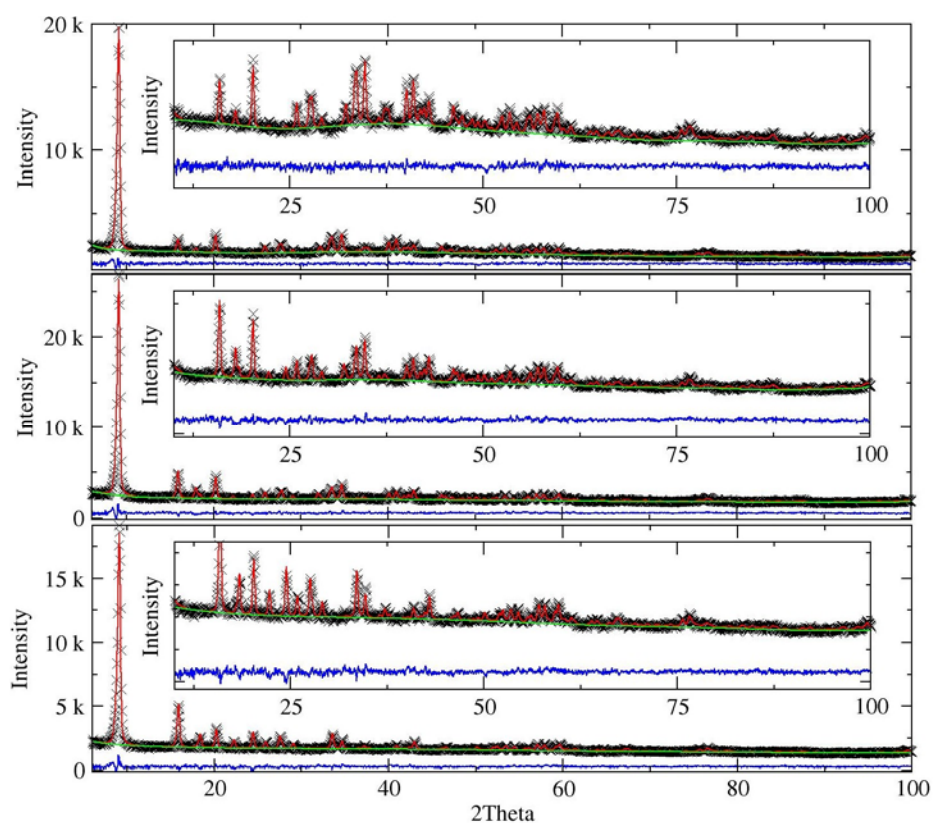
Figure S6. Neutron powder diffraction data and refinement of evacuated Mg_2(dobdc) (lower), after a dosing of 0.6 D_2 molecules per Mg^{2+} site (middle), and 1.2 D_2 molecules per Mg^{2+} site (upper). Green lines, crosses, and red lines represent the background, experimental, and calculated diffraction patterns, respectively. The blue line represents the difference between experimental and calculated patterns.
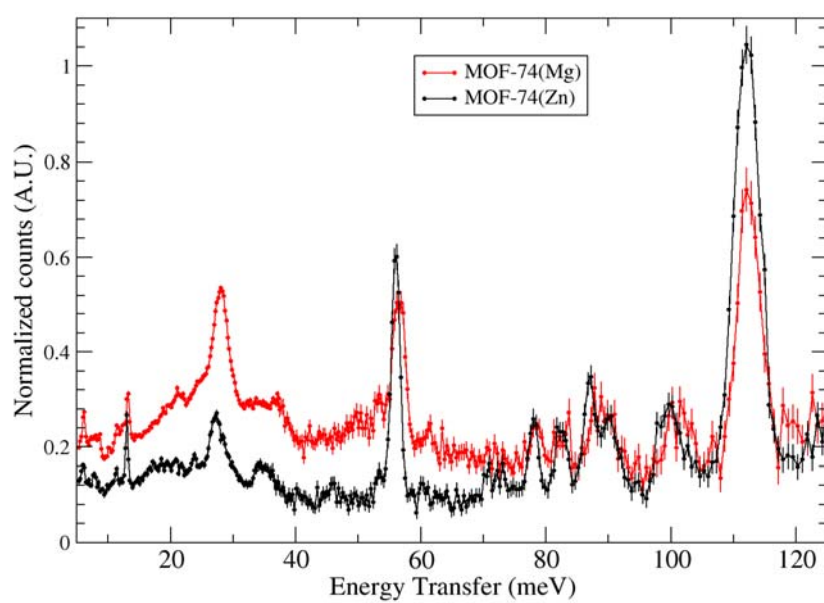
Figure S7. INS of $Mg_2(dobdc)$ (red) and $Zn_2(dobdc)$[7] (black) measured at 4 K on the FANS instrument. Vertical error bars indicate one standard deviation from counting statistics.
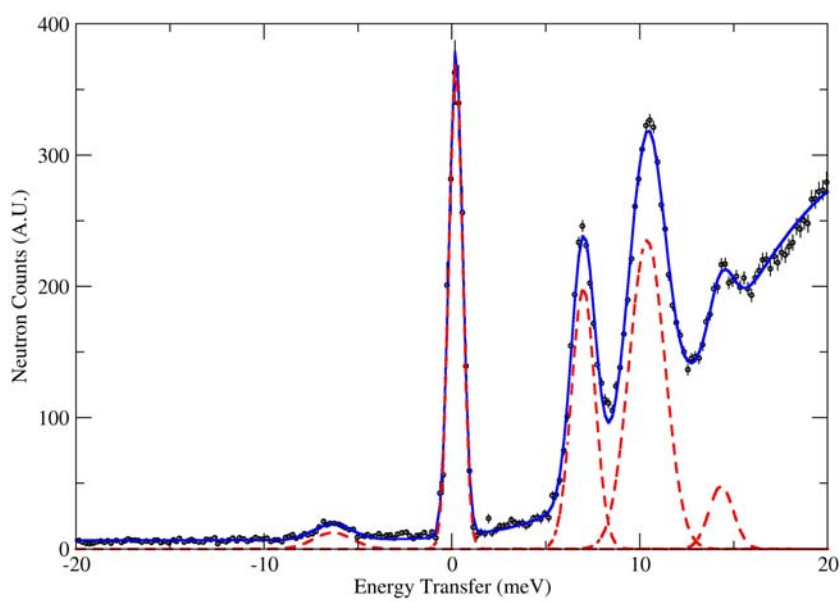
Figure S8. DCS data measured at 1.81 Å for 1.2 n-H_2 per Mg^{2+} site (black symbols) fit (blue line) to a series of Gaussian peaks (dashed red line) and a quadratic background. Vertical error bars indicate one standard deviation from counting statistics.
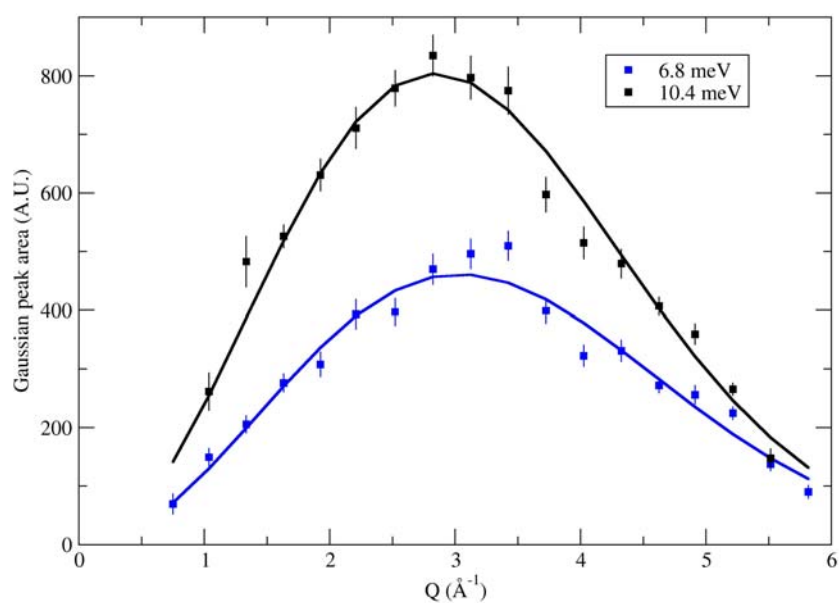
Figure S9. Extracted areas from fitting Gaussians to the Q-dependent DCS data. The Gaussian areas from the fits to the 6.8 meV (blue squares) and 10.4 meV (black squares) rotational transition peaks. The data are further fit to a model for hydrogen rotations (solid lines).[5] Vertical error bars show the estimated standard deviation from fitting the Gaussians to the data.
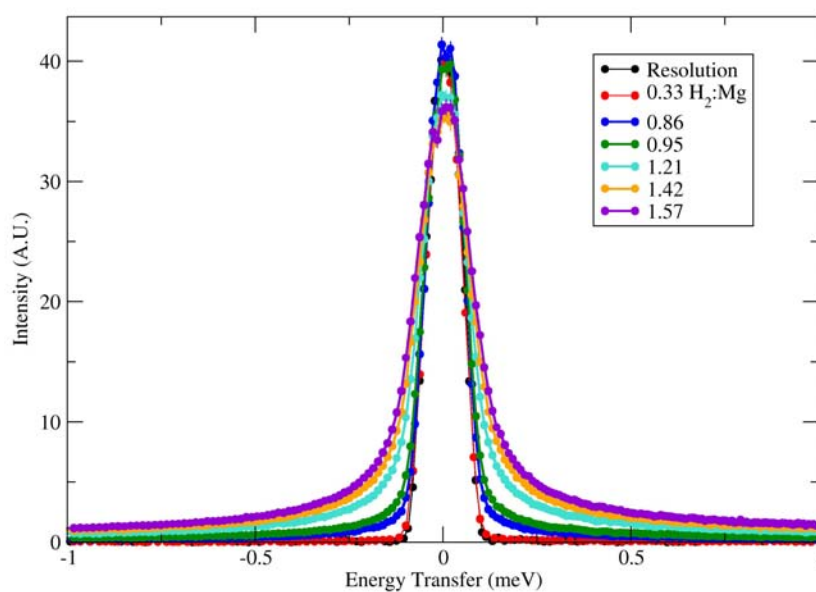
Figure S10. Q-summed data for all loadings indicating the magnitude of the quasielastic scattering as a function of loading at 77 K. The instrument resolution function was scaled to the elastic intensity of the substrate subtracted hydrogen-loaded data.
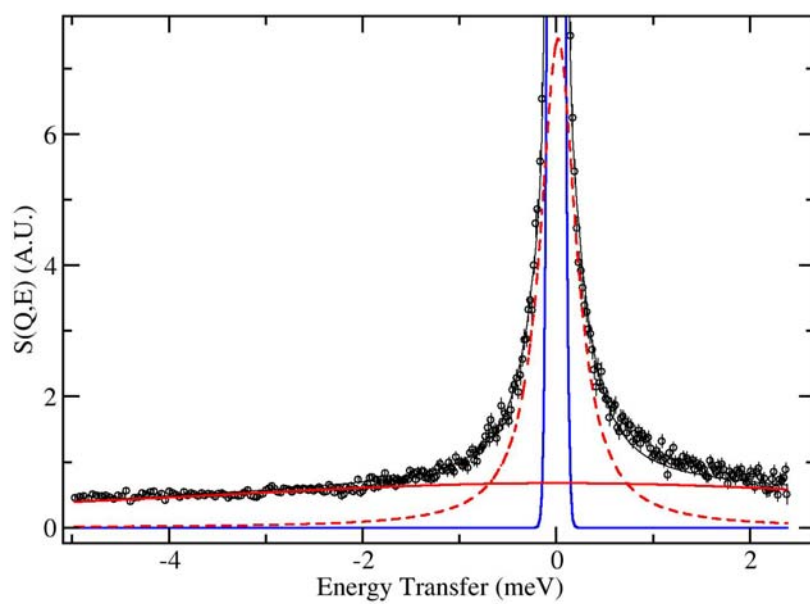
Figure S11. QENS data for a Q-slice (2.29 Å^{-1}) at a loading of 0.95 *n*-H$_2$ per Mg^{2+} site (black circles) with the bare material subtracted. Data (black line) are fit to a model comprising the resolution function (blue line), a narrow Lorentzian (dashed red line) and a broad Lorentzian (solid red line).
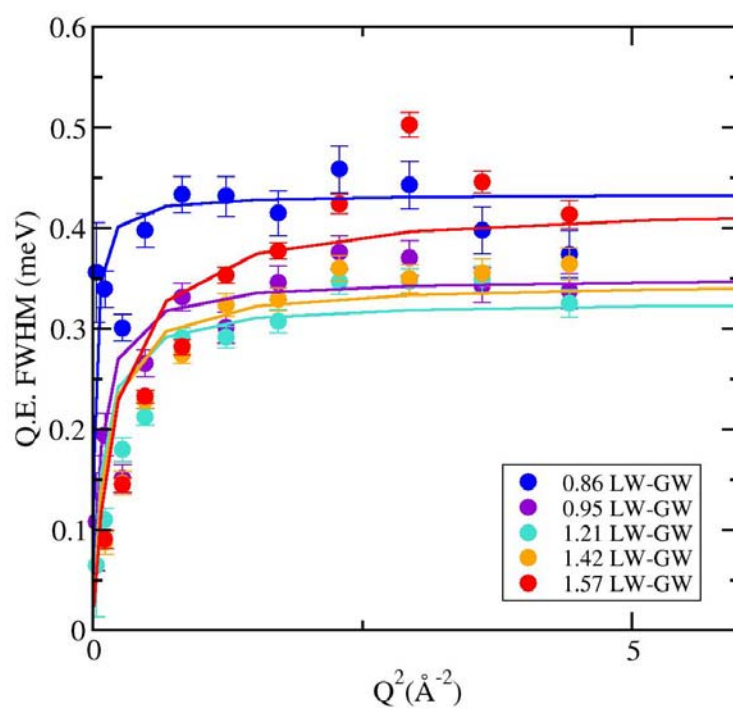
Figure S12. Full-width at half-maximum (FWHM) for the narrow Lorentzian component plotted against Q^2. Data at each loading are fit to the model of liquid-like jump diffusion described in the text.
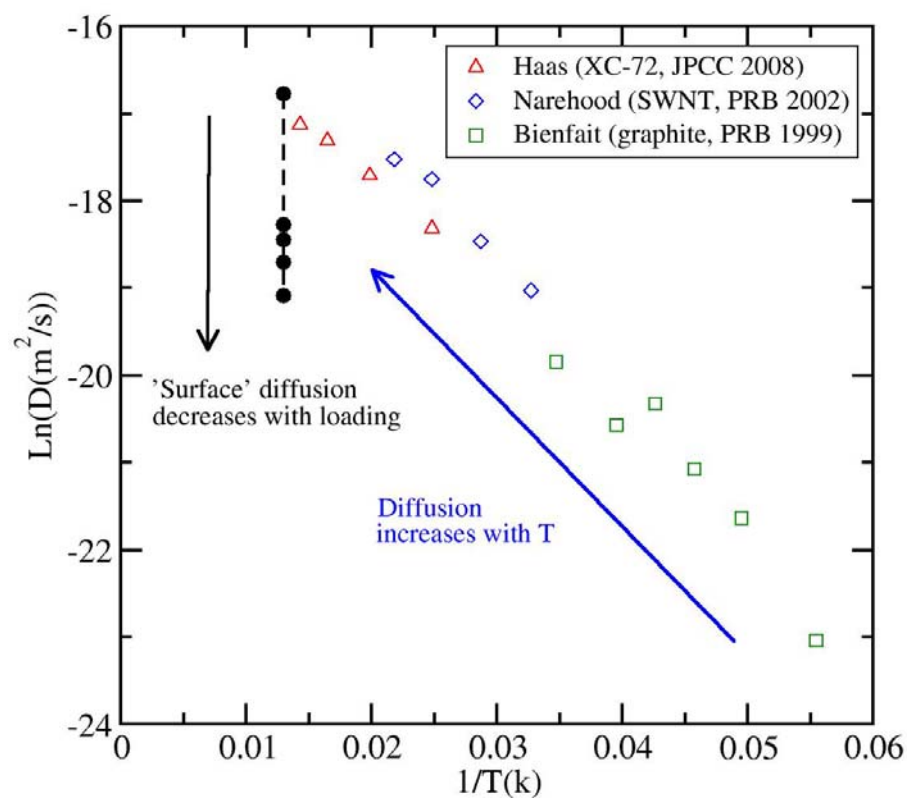
Figure S13. Diffusion parameter for the narrow Lorentzian component at 77 K with increasing loading (black circles). Data are compared to literature values for hydrogen diffusion on carbon surfaces of graphite,[13] single-walled nanotubes,[14] and XC-72 carbon.[15]
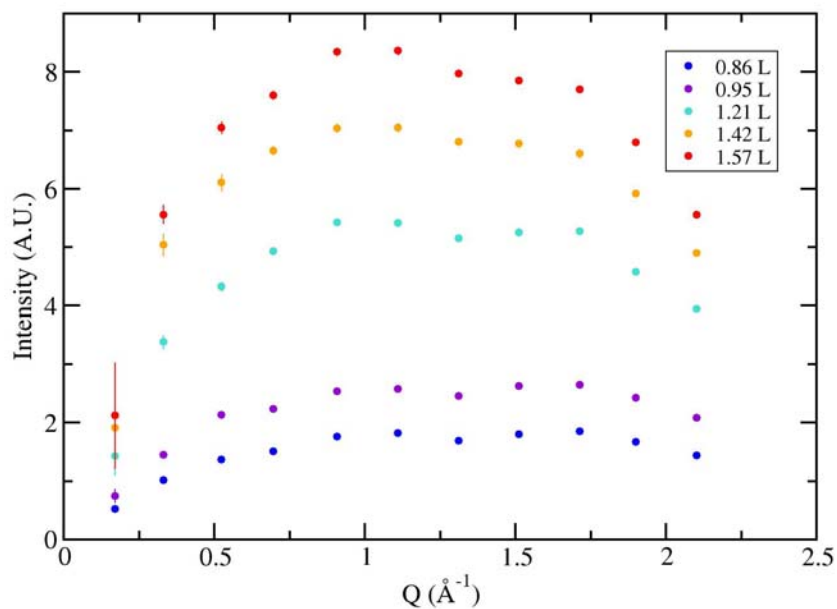
Figure S14. Areas for the narrow Lorentzian component of the fit to the QENS peak.
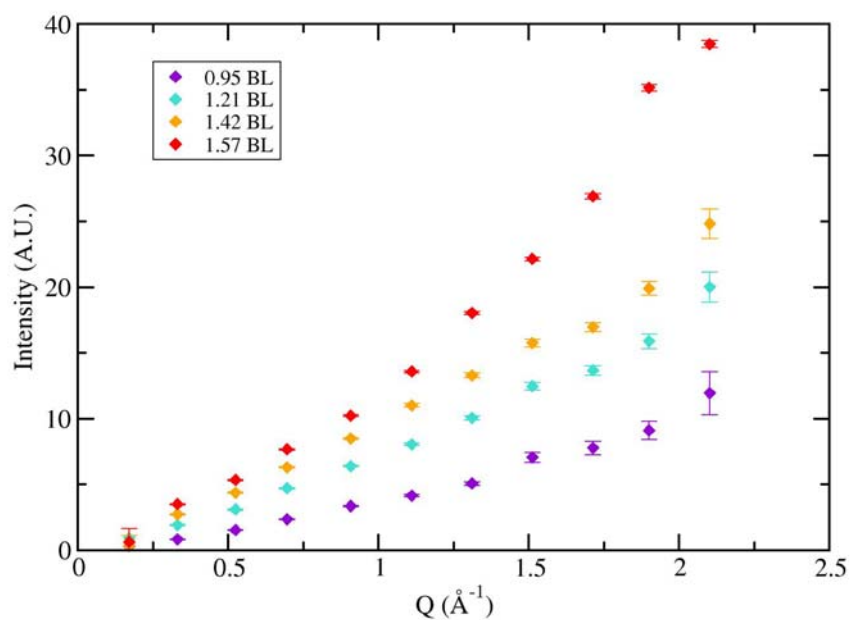
Figure S15. Areas for the broad Lorentzian component of the fit to the QENS peak..
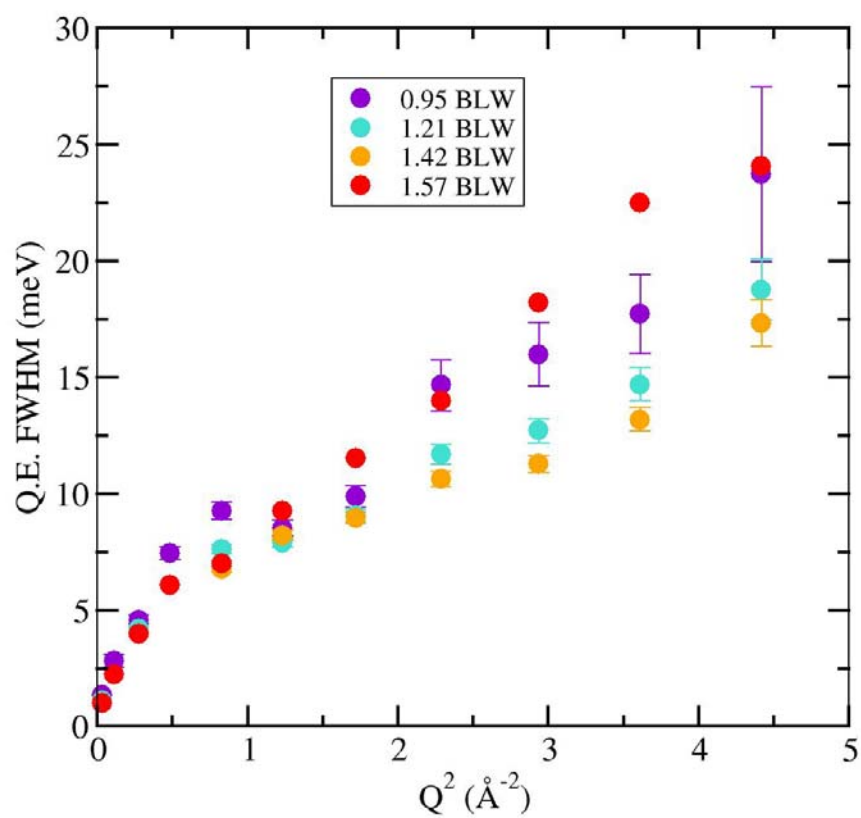
Figure S16. Extracted full-width at half-maximum (FWHM) for the broad Lorentzian plotted as a function of Q^2.

Mg(NO$_3$)$_2$·6H$_2$O

+

2,5-dihydroxyterephthalic acid
H$_4$dobdc

120 °C, 8 h
DMF/EtOH/H$_2$O

Mg$_2$(dobdc)
Honeycomb structure
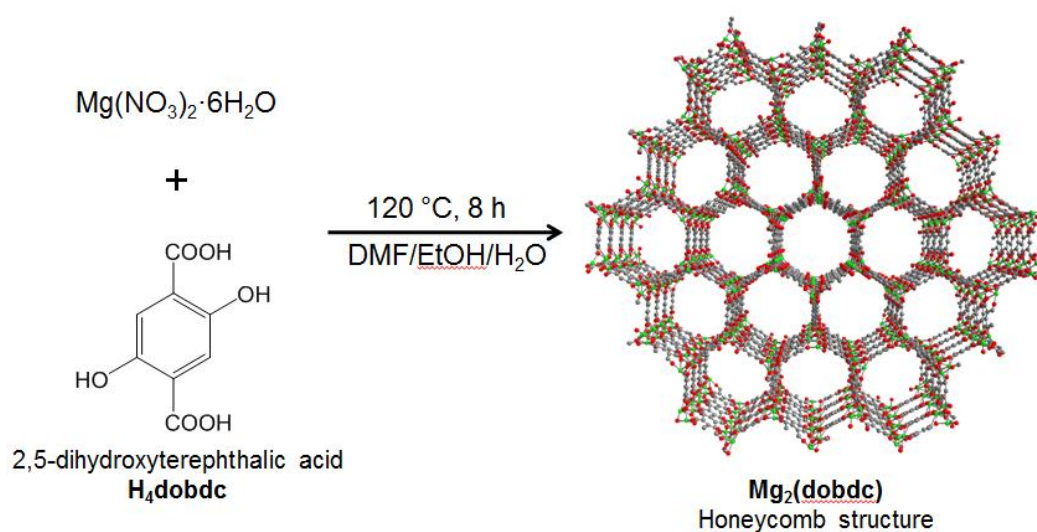
Scheme 1. Synthesis of Mg$_2$(dobdc), wherein Mg^{2+} ions and 2,5-dihydroxyterephthalic acid (H$_4$dobdc) are combined in solution to form a honeycomb-like structure with one-dimensional hexagonal channels. In the as-synthesized form, the Mg^{2+} ions are in an octahedral coordination environment with a sixth coordination site occupied by a solvent molecule. This solvent molecule is removed during activation to afford open Mg^{2+} adsorption sites.

References

(1)   S. R. Caskey, A. G. Wong-Foy, and A. J. Matzger, *J. Am. Chem. Soc.*, 2008, **130**, 10870.

(2)   E. Garrone and C. O. Arean, *Chem. Soc. Rev.*, 2005, **34**, 846.

(3)   J. G. Vitillo, L. Regli, S. Chavan, G. Ricchiardi, G. Spoto, P. D. C. Dietzel, S. Bordiga and A. Zecchina, *J. Am. Chem. Soc.*, 2008, **130**, 8386.

(4)   G. Spoto, J. G. itillo, D. Cocina, A. Damin, F. Bonino, and A. Zecchina, *Phys. Chem. Chem. Phys.*, 2007, **9**, 4992.

(5)   B. H. Toby, *J. Appl. Cryst.* 2001, **34**, 210.

(6)   Y. Liu, H. Kabbour, C. M. Brown, D. A. Neumann, and C. C. Ahn, *Langmuir,* 2008, **24**, 4772.

(7)   C. M. Brown, Y. Liu, T. Yildirim, V. K. Peterson, and C. J. Kepert, *Nanotechnology*, 2009, 204025.

(8)   T. J. Udovic, C. M. Brown, J. B. Leao, P. C. Brand, R. D. Jiggetts, R. Zeitoun, T. A. Pierce, I. Peral, J. R. D. Copley, Q. Huang, D. A. Neumann, and R. J. Fields, *Nuclear Inst. and Methods in Physics Research, A*, 2008, 588, 406.

(9)   R. T. Azuah, L. R. Kneller, Y. Qiu, P. L. W. Tregenna-Piggott, C. M. Brown, J. R. D. Copley, and R. M. Dimeo, *J. Res. Natl. Inst. Stan. Technol.*, 2009, **114**, 241.

(10)   J. R. D. Copley and J. C. Cook, *Chem. Phys.*, 2003, **292**, 477.

(11)   Accessible Surface Area Calculation Program, website address (August 2009): http://www.see.ed.ac.uk/~tduren/research/surface_area/.

(12)   A. K. Rappe, C. J. Casewit, K. S. Colwell, W. A. Goddard, and W. M. Skiff, *J. Am. Chem. Soc.*, 1992, **114**, 10024.

(13)   M. Bienfait, P. Zeppenfeld, R. C. Ramos, J. M. Gay, O. E. Vilches, and G. Coddens, *Phys. Rev. B*, 1999, **60**, 11773.

(14)   D. G. Narehood, J. V. Pearce, P. C. Eklund, P. E. Sokol, R. E. Lechner, J. Pieper, J. R. D. Copley, and J. C. Cook, *Phys. Rev. B*, 2003, **67**, 5.

(15)   O. E. Haas, J. M. Simon, S. Kjelstrup, A. L. Ramstad, and P. Fouquet, *J. Phys. Chem. C*, 2008, **112**, 3121.